Effects of the Atwood number on the Richtmyer-Meshkov instability in elastic-plastic media

Qian Chen,[1] Li Li,[1] Yousheng Zhang,[1,2,*] and Baolin Tian[1,2,†]
[1]*Institute of Applied Physics and Computational Mathematics, Beijing 100094, China*
[2]*Center for Applied Physics and Technology, Peking University, Beijing 100871, China*

(Received 23 September 2018; published 6 May 2019)

The Richtmyer-Meshkov instability of small perturbed single-mode interfaces between an elastic-plastic solid and an inviscid liquid is investigated by theoretical analysis and numerical simulation in this work. A modified model including the Atwood number effect is proposed to describe the long-term behaviors of small perturbations at the solid-liquid interface. In contrast to an effective theoretical model at the solid-vacuum interface, this model is appropriate at different Atwood numbers. Owing to the effect of elastic-plastic characteristics and the density ratio, the evolution of the spike amplitude exhibits nonlinear mechanical behavior. As the absolute value of the Atwood number decreases, the maximum spike amplitude also decreases. To validate this model, an Eulerian finite-difference multicomponent code is adopted to study the time evolution of the spike amplitude at different Atwood numbers. The model coefficients are obtained by analyzing the relevant characteristic statistics collected from the numerical results. Under different initial conditions such as Atwood number and shock strength, the applicability of this modified model is verified by comparing the numerical results with the model profile. The consistency in results signifies that the modified model is not only suitable for specific shock intensity and Atwood number, but also adaptable within a certain range.

DOI: 10.1103/PhysRevE.99.053102

I. INTRODUCTION

The Richtmyer-Meshkov (RM) instability describes the hydrodynamic phenomenon of an arbitrarily perturbed interface separating two materials with different properties when impulsively accelerated by a shock wave [1–6]. RM instability is often thought of as an impulsive or shock-induced version of the continuously driven Rayleigh-Taylor (RT) instability [7]. RT is induced when there is a mismatch between the density gradient and pressure ($\nabla\rho \cdot \nabla p < 0$) [7]. RM instability occurs whether the incident shock wave propagates from a light to a heavy medium ($\nabla\rho \cdot \nabla p < 0$) or from a heavy to a light fluid ($\nabla\rho \cdot \nabla p > 0$). In the case that an incident shock wave propagates from a heavy to a light fluid, phase reversal precedes the growth [5,7].

In the RM instability in an elastic-plastic medium, baroclinic effects are considered as the interpretation of the occurrence and development. The evolution of the tiny initial perturbations can be divided into several different conditions: linear growing stage, nonlinear growing stage and ejecta transition [8–11]. In the field of atomic physics and space science, experiments are designed to study the equation of state, transport properties, and implementation of the ejecta source at high-energy density matter [3,8,12]. When investigating the hydrodynamic instability in these experiments, it is found that the elastic-plastic media may remain in solid state during the shock loading process because the involved pressure is below the melting limit. The elastic-plastic constitutive properties of the solid must be considered when investigating the evolution of the interface between the solid and other media [13–16]. Exploring the role that the material property of the solid plays in the perturbation growth is essential to understanding the mechanism of the elastic-plastic RM instability. However, the measured characteristic statistics in RM instability can also be used as an indirect tool for evaluating the dynamic yield strength based on the theoretical model [17–21]. The elastic-plastic RM instability can be studied from the viewpoint of the fluid dynamics perspective, plasma physics, astrophysics, and solid mechanics [22,23]. Consequently, studying the elastic-plastic RM instability is meaningful in both academic research and application development. Considering that the relevant experiments are difficult and costly, numerical simulation approaches are adopted to study the RM instability in this work.

When a shock wave travels from a metal to a vacuum region, the shock wave first releases to zero pressure at the perturbation and reflects back to the metal as a rarefaction wave [8]. The shock wave interacts with the interface and causes the compression, inversion, and tension in perturbations [8]. Generally, the high-density substance propagates into the low-density substance to form spike structures and the low-density substance propagates into the high-density substance to form bubble structures. The initial conditions of the perturbations and physical parameters of the elastic-plastic medium both have significant influences on the interface evolution. Usually, $k\eta_0$ is used to characterize the initial condition of the single-mode perturbations, where k is the wave number of the perturbation and η_0 is the initial amplitude. With the growth of $k\eta_0$, the behavior of the interface at different stages can be qualitatively described as no spike growth, spike growth, and arrest, forming blunted RM tips and spike breakup resulting in ejecta transition [8,24]. The elastic-plastic medium has

*zhang_yousheng@iapcm.ac.cn
†tian_baolin@iapcm.ac.cn

unique properties that differ from fluid. If the yield stress Y of the elastic-plastic medium is quite small, the spike growth evolves similarly to that in a classical case in an ideal fluid. If there exists nonignorable yield stress in the solid medium, the amplitude of the spike will reach a maximum after a period of growth in the case of small perturbations. For the reason that the plasticity theory is intrinsically nonlinear, it was difficult to describe the interface evolution quantitatively [4,22,25,26]. Piriz *et al.* first discussed the long-term behavior of a light-heavy vacuum-solid interface [9,11]. They proposed an analytical model for the maximum spike amplitude of a small perturbed interface as a function of the initial perturbation conditions and physical parameters:

$$\eta_m^{\text{spike}} - \eta_0 = C\frac{\rho\dot{\eta}_0^2}{kY}, \tag{1}$$

where ρ is the density of the solid, $\dot{\eta}_0$ is the initial velocity, and C is a coefficient, the value of which is 0.29 in a light-heavy vacuum-solid interface [12,22,24]. Dimonte *et al.* studied the maximum spike amplitude in a heavy-light solid-vacuum interface. They modified the model by replacing the initial velocity by the maximum spike growth rate. The coefficient at this case is 0.24 and it is explained that the lower coefficient can be attributed to the phase-reversal process [24]. The analytical model for long-term behavior of the spike amplitude is the theoretical basis for evaluating the dynamic yield strength of solids [24].

The Atwood number, which is defined as $\mathrm{A} = (\rho_2 - \rho_1)/(\rho_2 + \rho_1)$, represents the density ratio of materials on the two sides of the interface. Current research on elastic-plastic RM instability mainly focuses on the solid-vacuum interface, i.e., $|\mathrm{A}| = 1$ [23,27–29]. Meanwhile, the solid-liquid interfaces exist extensively in practical applications. Building an Atwood number dependent model for perturbation growth can contribute to a better understanding of elastic-plastic RM instability and to optimal designs in weapon physics [30]. In the classic fluidic RM instability, Zhang and Guo have already studied all spikes and bubbles at any density ratio closely following a universal curve in terms of scaled dimensionless variables [30]. In the elastic-plastic Rayleigh-Taylor instability, Piriz *et al.* adequately illustrated the perturbation growth at solid-liquid interfaces of different densities [31–38]. At the Cu-Al interface, it is found that the influence of yield stress and initial perturbations on the interface evolution is similar to that at solid-vacuum interface [39]. Solids undergoing large deformations in contact with fluids occur in several engineering contexts including implosion and penetration [39]. During the implosion, the pusher remains in a solid state, conserving strength properties, while the absorber is melted, remaining in a liquid state [27,31]. In the experiments on magnetically imploded liners, the metal shell can be partially or totally melted depending on the intensity and time history of the electrical current [15,27]. In these views, a solid-liquid interface is a common configuration in engineering applications. The investigation of the perturbation growth at solid-liquid interfaces of different densities is necessary and practical in engineering. However, relevant research on the Atwood number effects in the elastic-plastic RM instability is not sufficient. This work is aimed at proposing a modified model of the perturbation growth at a solid-liquid interface at different Atwood numbers.

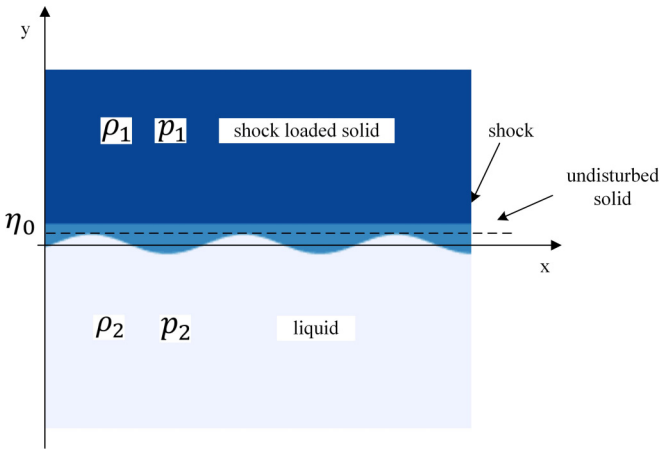

FIG. 1. Schematic of the solid-liquid interface.

In this paper, the RM instability of the small perturbed single-mode interfaces between an elastic-plastic solid and an inviscid liquid is systematically examined at different Atwood numbers. By theoretically analyzing the stress condition of the interface, the motion equation for the interface is built based on Newton's second law. Then, the maximum spike amplitude model with two undetermined model coefficients is proposed. A numerical simulation is adopted to verify the model and obtain the model coefficients. Further, the applicability of this modified model is verified by comparing the numerical results with the model profile under different initial conditions such as Atwood number and shock speed. The consistency of the theoretical prediction and numerical results is satisfactory. Therefore, this model can be used to describe the Atwood number dependent spike growth in the RM instability for small perturbations.

II. MODIFIED MODEL OF PERTURBATION GROWTH AT DIFFERENT ATWOOD NUMBERS

The elastic-plastic RM instability at the solid-liquid interface is considered theoretically in this section. An analytical model is proposed to describe the evolution of small perturbations at different Atwood numbers. The theoretical analysis is based on the work of Piriz *et al.* [10,12,27,34,35] investigating the RM instability in elastic-plastic media at the solid-vacuum interface ($\mathrm{A} = 1$). The effect of density ratio is introduced by an Atwood function, which can make the model appropriate for solid-liquid interface at different Atwood numbers.

A schematic of the interface is shown in Fig. 1. A medium with elastic-plastic properties is located in the semispace $y < 0$ and the inviscid liquid is located in the semispace $y > 0$. The upper area is the solid material that the shock wave has already traveled through while the middle area represents the undisturbed solid. At the interface of the solid and liquid, there is a small sinusoidal perturbation characterized by the wavelength λ, the initial amplitude η_0, and the perturbation wave number k ($k = 2\pi/\lambda$). In the case of small perturbations, the wave number and initial amplitude should satisfy the relationship $k\eta_0 \ll 1$. The effect of the interaction between

the shock wave and the solid-liquid interface generates a rotational velocity field inside the shock compressed material. Before the solid material melts, the effect of the rotation velocity field in liquid on solid media is relative weak. Transmitted and reflected shocks have traveled sufficiently far, compared to the wavelength of the perturbations. Baroclinic effects contribute to the early-time, or small-amplitude linear growth of the instability before nonlinear developments of the perturbation. Therefore, the shock wave reflections are ignored in the limit of small perturbations and weak shock [12,40,41]. The details of the interaction between the shock wave and the solid-liquid interface are ignored. At $t = 0$, the shock wave has already traveled through the interface and propagates into the liquid semispace. In the weak shock limit, the impulsive model of Richtmyer denotes that the velocity of interface is $k\eta_0\Delta u\mathrm{A}$ in the linear regime [2], where Δu denotes the interface velocity jump and A is the Atwood number. This linear perturbation growth rate $k\eta_0\Delta u\mathrm{A}$ at fluid interfaces is considered as the initial velocity of the elastic-plastic RM instability at $t = 0$. After the shock wave propagates far into the undisturbed area, the particle velocity decays exponentially as $e^{ky}(y < 0)$ with the distance from the interface. Therefore, the velocity field can be approximated in the following form corresponding to an ideal inviscid fluid:

$$\dot{\eta} = v_y = \dot{\xi}(t)e^{ky}\sin kx, \tag{2}$$

where $\dot{\xi}(t)$ is the instantaneous normal velocity at the interface. Therefore, the amplitude is written as

$$\eta = \xi(t)e^{ky}\sin kx, \tag{3}$$

A Prandtl-Reuss rule with the von Mises yield stress criterion [42,43] is used to get a convenient expression for the deviatoric part S_{ij} of the stress tensor $\sigma_{ij} = -p\delta_{ij} + S_{ij}$, where p is the thermodynamic pressure and δ_{ij} is the Kronecker tensor [12].

$$\begin{aligned}
&\dot{S}_{ij} + 2GS_{ij}\frac{S_{mn}D_{mn}}{S_{mn}S_{mn}} \\
&\quad = 2GD_{ij}, \quad S_{ij}D_{ij} > 0 \ \text{ and } \ S_{ij}S_{ij} = \frac{2}{3}Y^2, \quad \text{plastic}, \\
&\dot{S}_{ij} = 2GD_{ij}, \quad S_{ij}D_{ij} < 0 \ \text{ and } \ S_{ij}S_{ij} < \frac{2}{3}Y^2, \quad \text{elastic},
\end{aligned} \tag{4}$$

where G is the solid shear modulus and Y is the solid yield stress. The elastic limit of the solid material is ξ_p. After the shock wave travels through the interface, the stresses produced by the interaction between the shock wave and perturbations cause the deformation of the solid material. The perturbations compress, invert, and then grow in tension into the liquid region forming the spike structure. In this procedure, the deformation of solid material gradually grows larger than the elastic limit. The later evolution of the spike takes place within the plastic state. According to previous work of Piriz *et al.*, the normal component S_{yy} of the deviatoric part of the stress tensor is written as [12,34]

$$S_{yy} = \begin{cases} 2kG\xi e^{ky}\sin kx, & \xi \leqslant \xi_p \\ \frac{1}{\sqrt{3}}Y\sin kx, & \xi \geqslant \xi_p \end{cases}. \tag{5}$$

Taking a voxel in the interface into consideration, the cross-sectional area of the voxel is D. The motion of interface is associated with the voxel. When the shock travels through the solid-vacuum interface, it is assumed that only the fluid within a distance $a = \frac{l}{k}$ participates in the motion in the linear regime. In the same shock intensity, the length of the voxel is assumed to be inversely proportional to the total density of the materials. Considering that the development of the interface can be seen as the process of shock-accelerating media, the value of a is assumed to be inversely proportional to the total density of the materials. Therefore, we can get that

$$a = \frac{l}{k}\frac{\rho_s}{\rho_1 + \rho_2}, \tag{6}$$

where ρ_s is the density of the solid; ρ_1 and ρ_2 are the densities of the material on each side of the interface. For the reason that it cannot be determined whether the shock wave travels from solid to liquid or from liquid to solid in this section, ρ_s is used instead of ρ_1 or ρ_2. l is a dimensionless parameter related to length. In the linear stage, the evolution of the interface is approximately symmetrical.

In the evolution of the interface, the voxel is subjected to thermodynamic pressure and solid stress. In the case of a small perturbation, the external force that is applied on the voxel in the normal direction can be written as

$$F_y = \left(F_{p_1} + F_{p_2}\right) - S_{yy}D, \tag{7}$$

where p_1 and p_2 are the thermodynamic pressures on each side of the interface; F_{p_1} and F_{p_2} are forces caused by the thermodynamic pressure. D is the cross-sectional area. Under the pressure balance assumptions, thermodynamic pressure satisfies the relationship $P_1 = P_2$ and $F_{p_1} + F_{p_2} = 0$. Based on the force analysis, the motion equation of the voxel can be obtained based on Newton's second law:

$$(\rho_1 aD + \rho_2 aD)\ddot{\eta} = -S_{yy}D. \tag{8}$$

This equation can be further written as

$$(\rho_1 a + \rho_2 a)\ddot{\xi} = \begin{cases} -2kG\xi, & \xi \leqslant \xi_p \\ -\frac{1}{\sqrt{3}}Y\frac{1}{e^{ky}}, & \xi \leqslant \xi_p \end{cases}. \tag{9}$$

The maximum amplitude of the spike can be obtained in three steps: the elastic state, the transient time when the solid material transforms from the elastic state to the plastic state, and the plastic state. In the elastic state, the deformation of the solid is below the elastic limit ξ_p. The motion equation can be reduced to the following form:

$$\ddot{\xi}_1(t) + \frac{2kG\xi_1(t)}{(\rho_1 + \rho_2)a} = 0. \tag{10}$$

During the process when the shock wave travels through the interface ($t = 0$), it is assumed that there is no deformation near the interface and so the elastic-plastic property can be ignored. Therefore, the initial growth rate of the interface agrees with the linear growth rate of the impulsive model for the fluidic RM instability [2]. At $t > 0$, the growth rate of the spike amplitude decreases because of the elastic-plastic property and then the interface evolution exhibits nonlinear mechanical behavior. The initial conditions can then be

written as $\xi_1(0) = 0, \dot{\xi}_1(0) = u_0 = k\eta_0 \Delta u \mathrm{A}$. Under these circumstances, we can get the solution of $\xi_1(t)$ as

$$\xi_1(t) = \sqrt{\frac{a(\rho_1+\rho_2)}{2kG}} u_0 \sin\left[\sqrt{\frac{2kG}{a(\rho_1+\rho_2)}} t\right], \tag{11}$$

$$\dot{\xi}_1(t) = u_0 \cos\left[\sqrt{\frac{2kG}{a(\rho_1+\rho_2)}} t\right]. \tag{12}$$

To simplify the expressions, we introduce a parameter τ given by

$$\tau = \sqrt{\frac{a(\rho_1+\rho_2)}{2kG}}, \tag{13}$$

so that the expressions for $\xi_1(t)$ and $\dot{\xi}_1(t)$ can be reduced to the following forms:

$$\xi_1(t) = \tau u_0 \sin\left(\frac{t}{\tau}\right), \quad \dot{\xi}_1(t) = u_0 \cos\left(\frac{t}{\tau}\right). \tag{14}$$

The transient time when the solid material transforms from the elastic state to the plastic state is needed to determine the initial conditions in the plastic state. According to the continuum hypothesis, the elastic limit ξ_p satisfies the relationship

$$-2kG\xi_p = -\frac{1}{\sqrt{3}} Y e^{-ky}. \tag{15}$$

In the case of small perturbation, the value of $-ky$ is relatively small. To simplify the subsequent part of the solution process, it is assumed that the value of e^{-ky} is proportional to the value of e^{-ky_p} (the scale factor being m), and y_p is associated with the length of the spike. Similar to the research method in the previous work of Piriz *et al.* [33–35], the average motion of a region is affected by the instability which extends up to a distance of the order of k^{-1} from the interface. The onset of the plastic flow is not expected to be felt until plastic flow has affected the entire region with the thickness of the order k^{-1}. In order to simplify the solution process, we decide not to give a precise account of the motion equation. Therefore it is reasonable to approximately give the value of its average behavior over the region of thickness k^{-1} and evaluate the equation at $y_p = k^{-1}$ in the solid-vacuum case. When considering the effects of density ratio, the expression of y_p is similar to that of a:

$$y_p = \frac{n}{k} \frac{\rho_s}{\rho_1+\rho_2}. \tag{16}$$

Similar to l, n is also a dimensionless parameter related to length. In the subsequent analysis, e^{-ky} is simply recorded as b, so that the elastic limit is $\xi_p = Yb/2\sqrt{3}kG$. By using the solution of $\xi_1(t)$, the transient time t_p when the solid material transforms from the elastic state to the plastic state can be calculated as

$$t_p = \tau \arcsin\left(\frac{bY}{2\sqrt{3}kGu_0\tau}\right). \tag{17}$$

In the plastic state, the spike amplitude grows larger than the elastic limit. The motion equation in this state can be written as

$$\ddot{\xi}_2(t) + \frac{Yb}{\sqrt{3}a(\rho_1+\rho_2)} = 0. \tag{18}$$

If it is assumed that the deformation and deformation rate are continuous when the solid material transforms from the elastic state to the plastic state, the initial conditions in this state are

$$\xi_1(t_p) = \xi_2(t_p) = \xi_p, \tag{19}$$

$$\dot{\xi}_1(t_p) = \dot{\xi}_2(t_p) = u_0 \cos\left[\arcsin\left(\frac{Yb}{2\sqrt{3}kGu_0\tau}\right)\right] = u_0\sqrt{1 - \frac{Y^2b^2}{12k^2G^2u_0^2\tau^2}}. \tag{20}$$

By integrating the motion equation in the plastic state from $t = t_p$, the evolution of $\xi_2(t)$ is obtained as follows:

$$\dot{\xi}_2(t) - \dot{\xi}_2(t_p) = -\frac{Yb}{\sqrt{3}a(\rho_1+\rho_2)}(t - t_p), \tag{21}$$

$$\xi_2(t) - \xi_2(t_p) = -\frac{Yb}{2\sqrt{3}a(\rho_1+\rho_2)}(t - t_p)^2 + \dot{\xi}_2(t_p)(t - t_p). \tag{22}$$

If the amplitude of the spike reaches its maximum value at $t = t_m$, the first-order time derivative of the spike length is zero at that time; i.e., $\dot{\xi}_{\max}(t_m) = 0$. Furthermore, the following equation can be obtained.

$$\xi_{\max} - \xi_2(t_p) = \frac{\sqrt{3}}{2}\frac{a}{b}\frac{1}{Y}(\rho_1+\rho_2)\left(u_0^2 - \frac{Y^2b^2}{12k^2G^2\tau^2}\right). \tag{23}$$

By rearranging the above equations, we can get

$$\xi_{\max} = \frac{Y}{4\sqrt{3}kG}b + \frac{\sqrt{3}}{2}\frac{a}{b}\frac{(\rho_1+\rho_2)u_0^2}{Y} = \frac{Y}{4\sqrt{3}kG}b + \frac{\sqrt{3}}{2}\frac{a}{b}(\rho_2-\rho_1)A\frac{(k\eta_0\Delta u)^2}{Y}. \tag{24}$$

Therefore, the expression of $k\eta_{\max}$ can be obtained as follows:

$$k\eta_{\max} = \frac{Y}{4\sqrt{3}G} + \frac{\sqrt{3}}{2}\frac{ka}{b^2}(\rho_2-\rho_1)\mathrm{A}\frac{(k\eta_0\Delta u)^2}{Y}. \tag{25}$$

Given the relationship between ρ_1, ρ_2, ρ_s and the Atwood number,

$$\frac{\rho_s}{\rho_1+\rho_2} = \frac{1+|\mathrm{A}|}{2}, \tag{26}$$

combined with the expressions for a and b, the expression for $k\eta_{\max}$ can be rewritten as

$$k\eta_{\max} = \frac{Y}{4\sqrt{3}G} + \frac{\sqrt{3}}{2}l\rho_s n^2\left(1 + m\frac{1+|\mathrm{A}|}{2}\right)^2 \mathrm{A}^2\frac{(k\eta_0\Delta u)^2}{Y}. \tag{27}$$

By merging the dimensionless numbers and introducing parameters α and β, the final expression for $k\eta_{\max}$ is

$$k\eta_{\max} = \frac{Y}{4\sqrt{3}G} + \alpha(\beta|\mathrm{A}| + \beta + 2)^2\rho_s \mathrm{A}^2 \frac{(k\eta_0\Delta u)^2}{Y}. \quad (28)$$

The following auxiliary function $f(\mathrm{A})$ dependent on the Atwood numbers is introduced to represent the effect of density ratio on the spike growth.

$$f(\mathrm{A}) = \alpha(\beta|\mathrm{A}| + \beta + 2)^2\mathrm{A}^2, \quad (29)$$

$$k\eta_{\max} = \frac{Y}{4\sqrt{3}G} + f(\mathrm{A})\frac{\rho_s(k\eta_0\Delta u)^2}{Y}. \quad (30)$$

In the next section, numerical simulations are conducted to study the variation of the spike maximum amplitudes under different Atwood numbers, and then estimate the values of the parameters α and β.

III. NUMERICAL VALIDATION OF THE MODIFIED MODEL

A. Numerical framework

An Eulerian finite-difference multicomponent code is adopted in this work. In the Eulerian frame of Cartesian coordinates, the conservation equations for mass, momentum, energy, deformation gradient tensor, and volume fraction are, respectively, as follows:

$$\begin{aligned}
\frac{\partial\rho}{dt} + \frac{\partial\rho u_i}{\partial x_i} &= 0,\\
\frac{\partial\rho u_i}{\partial t} + \frac{\partial(\rho u_i u_j - \sigma_{ij})}{\partial x_j} &= 0,\\
\frac{\partial\rho E}{\partial t} + \frac{\partial(\rho E u_j - \sigma_{ij}u_i)}{\partial x_j} &= 0,\\
\frac{\partial g^e_{ij}}{\partial t} + \frac{\partial u_{k}{}^{e}_{ik}}{\partial x_j} &= u_k\left(\frac{\partial g^e_{ik}}{\partial x_j} - \frac{\partial g^e_{ij}}{\partial x_k}\right) + L^p_{ik}g^e_{kj},\\
\frac{\partial\alpha}{\partial t} + u_k\frac{\partial\alpha}{\partial x_k} &= 0,
\end{aligned} \quad (31)$$

where $\rho, u_i, E, \sigma_{ij}, \alpha$ are density, x_i coordinate velocity, total energy, Cauchy stress, and volume fraction, respectively g_{ij} is the inverse deformation tensor defined as $g_{ij} = \partial X_i/\partial x_j$. X and x are coordinates in the Lagrangian and Eulerian frames of reference. In the deformation gradient tensor equation, the tensor L^p_{ik} reflects the influence of the plastic effect on the elastic deformations and can be modeled in the following form:

$$\begin{aligned}
L^p_{ik} &= \frac{1}{\tau_{\mathrm{rel}}}g^e_{im}\sigma'_{mn}(g^e)^{-1}_{nk},\\
\frac{1}{\tau_{\mathrm{rel}}} &= \frac{1}{2\mu(\rho/\rho_0)\tau_0}\left[\frac{H\left(\sigma'_{ij}\sigma'_{ij} - \frac{2}{3}\sigma_Y^2\right)}{\mu^2}\right].
\end{aligned} \quad (32)$$

Here $\sigma'_{ij} = \sigma_{ij} - \sigma_{kk}\delta_{ij}/3$ is the deviatoric Cauchy stress, τ is the relaxation time, and μ is the shear modulus of solid materials. $H(\cdots)$ is the Heaviside function and is used to determine whether the solid material is in the plastic state. When the yield criterion $\sigma'_{ij}\sigma'_{ij} - 2/3\sigma_Y^2 > 0$ is satisfied, the plastic effect should be considered. A diffuse interface model based on the volume fraction was introduced to solve the problem of multimedia mixing. The whole flow field is regarded as the mixing region. Mixing density ρ, Cauchy stress σ, pressure p, internal energy ε^h, and elastic energy ε^e can be well defined by the volume fraction. The mixing model based on volume fraction is shown in the following.

$$\begin{aligned}
\rho &= \alpha_1\rho_1 + \alpha_2\rho_2, \quad \sigma = \alpha_1\sigma_1 + \alpha_2\sigma_2,\\
\rho\varepsilon^h &= \alpha_1\varepsilon^h_1 + \alpha_2\varepsilon^h_2, \quad \rho\varepsilon^e = \alpha_1\varepsilon^e_1 + \alpha_2\varepsilon^e_2,\\
p &= (\rho\varepsilon^h - B)/A,
\end{aligned} \quad (33)$$

where the subscripts 1 and 2 represent material 1 and material 2, respectively. A and B are corresponding coefficients related to the equation of state. In this paper, the time scheme is a third-order Runge-Kutta method and the differential scheme used in space is the fifth-order accurate weighted essentially non-oscillatory (WENO5) scheme.

Under a shock wave, the Mie-Gruneisen equation of state is adopted to characterize both the solid and the liquid [13,22,44]. In the simulation, the solid material is set to be copper while the liquid is set to be water. The Atwood number is adjusted by changing the density of the liquid. Then the evolution of small perturbation of the interface undergoing the elastic-plastic RM instability at different Atwood numbers is investigated. To avoid influences caused by the thermodynamic parameters, the density of the liquid varies while the thermodynamic parameters of the liquid remain consistent with water in the different numerical cases. The simulation parameters of copper and liquid are listed in Table I.

TABLE I. Simulation parameters of copper and liquid

	Copper	Liquid
ρ (kg/m^3)	8900	1–3000
c_0 (m/s)	3940	1480
s	1.49	2.56
γ	2.02	0.4934
Y (MPa)	500	
G (GPa)	39.38	

B. Verification of the simulation program

To verify the correctness of the simulation code, the numerical results are compared with the conclusions in the literature [24]. As shown in Fig. 2, the initial conditions are in accordance with the configurations in Ref. [24]. A shock is produced in copper by means of setting up a Riemann problem. The shock moves toward a perturbed interface within solid. Shock speed is 7640 m/s. Two-dimensional (2D) single-mode perturbations ($k\eta_0 = 0.125$) are located at the interface of the copper and the gas. The density of the copper is 8900 kg/m^3 and the density of the gas is 1 kg/m^3. In the simulation of this part, we use one wavelength $\lambda \equiv 2\pi/k =$ 4.3 cm with 100 zones/λ for numerical convergence. The size of the computational domain is 4.3 cm × 8.6 cm and it is paved with $N_x \times N_y = 100 \times 900$ cells. For the reason that the variations of elastic-plastic flow in the Y coordinate is mainly

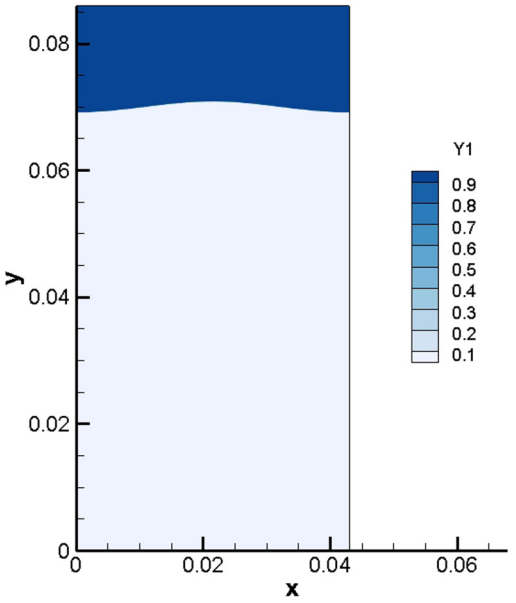

FIG. 2. The initial flow field accordance with that in Ref. [24].

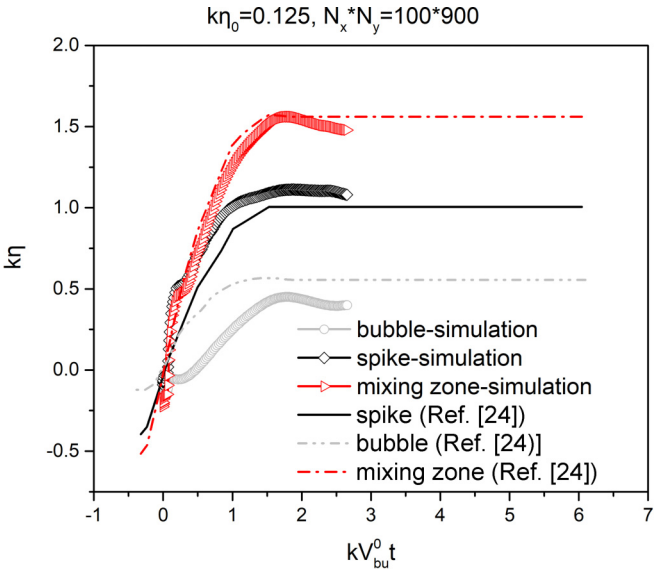

FIG. 3. Simulated evolution of the width of the mixing zone, spike amplitude, and bubble amplitude compared with that in Ref. [24].

discussed in this manuscript, we only refine the grids in the Y direction in order to reduce the computing time. Meanwhile, we have checked that the numerical results are convergent at this mesh quantity. The boundary conditions at the left and right sides are periodic. For the accuracy of the verification process, the initial simulation condition is set to be the same as that in the literature [24]. After the shock wave travels through the interface, the velocity acquired by the interface is used as background velocity. Then, the initial velocity of all regions will be changed by reducing the estimated interface velocity. In this way, the mean position of the interface will approximately remain in the computational domain with the development of the interface [23]. The position of the mixing zone is differentiated by volume fraction thresholds. Some characteristic statistics such as spike amplitude and bubble amplitude are collected.

By comparing the numerical results with those in the literature, it is found that the profile of the width of the mixing zone as a function of time is almost the same as that in the literature. Meanwhile, the maximum length of the spike and bubble are close to the reference solution and the amplitude evolution of the spike and bubble are consistent (Fig. 3). That is, the numerical results for the linear perturbation growth of the RM instability are trustworthy. Therefore, it is reasonable to use this code to further research the evolution of the interface undergoing elastic-plastic RM instability at small perturbations.

C. Numerical results at different Atwood numbers

Given that the correctness of the simulation code has been verified, we can adopt this code to investigate the evolution of the small perturbed interface at different Atwood numbers. The relevant characteristic statistics are collected and compared with the model results of Eq. (28). The undetermined model coefficients α and β are estimated by using the numerical results at different Atwood numbers. In addition to the density of the liquid substance, other simulation parameters remain invariable during the numerical process. For different numerical cases, the densities of the materials on both sides of the interface and the corresponding Atwood numbers are listed in Table II. The setting of the initial flow field is almost the same as that of Sec. III B, except that the substance in the low-density region changes from gas to liquid of different densities. The 2D single-mode perturbations ($k\eta_0 = 0.125$) are located at the interface of copper and liquid. The wavelength of the perturbation is also 4.3 cm. The density of the solid is 8900 kg/m^3 and the density of the liquid varies in the range of 1 kg/m^3–3000 kg/m^3. The variation of liquid density is determined through numerical tests. When the density of the liquid is larger than 3000 kg/m^3, the perturbation growth is relatively slow and the changes of the maximum spike length are small at different Atwood numbers. In this section, the most important characteristic statistic is the spike's maximum amplitude. The liquid is considered inviscid in the numerical process.

TABLE II. Densities and Atwood numbers at different numerical cases.

Case	ρ_1 (kg/m^3)	ρ_2 (kg/m^3)	Atwood	Postshock Atwood
1	8900	100	−0.978	−0.976
2	8900	300	−0.935	−0.929
3	8900	500	−0.894	−0.884
4	8900	700	−0.854	−0.842
5	8900	1000	−0.798	−0.782
6	8900	1500	−0.712	−0.691
7	8900	2000	−0.633	−0.609
8	8900	2500	−0.561	−0.536
9	8900	3000	−0.496	−0.469

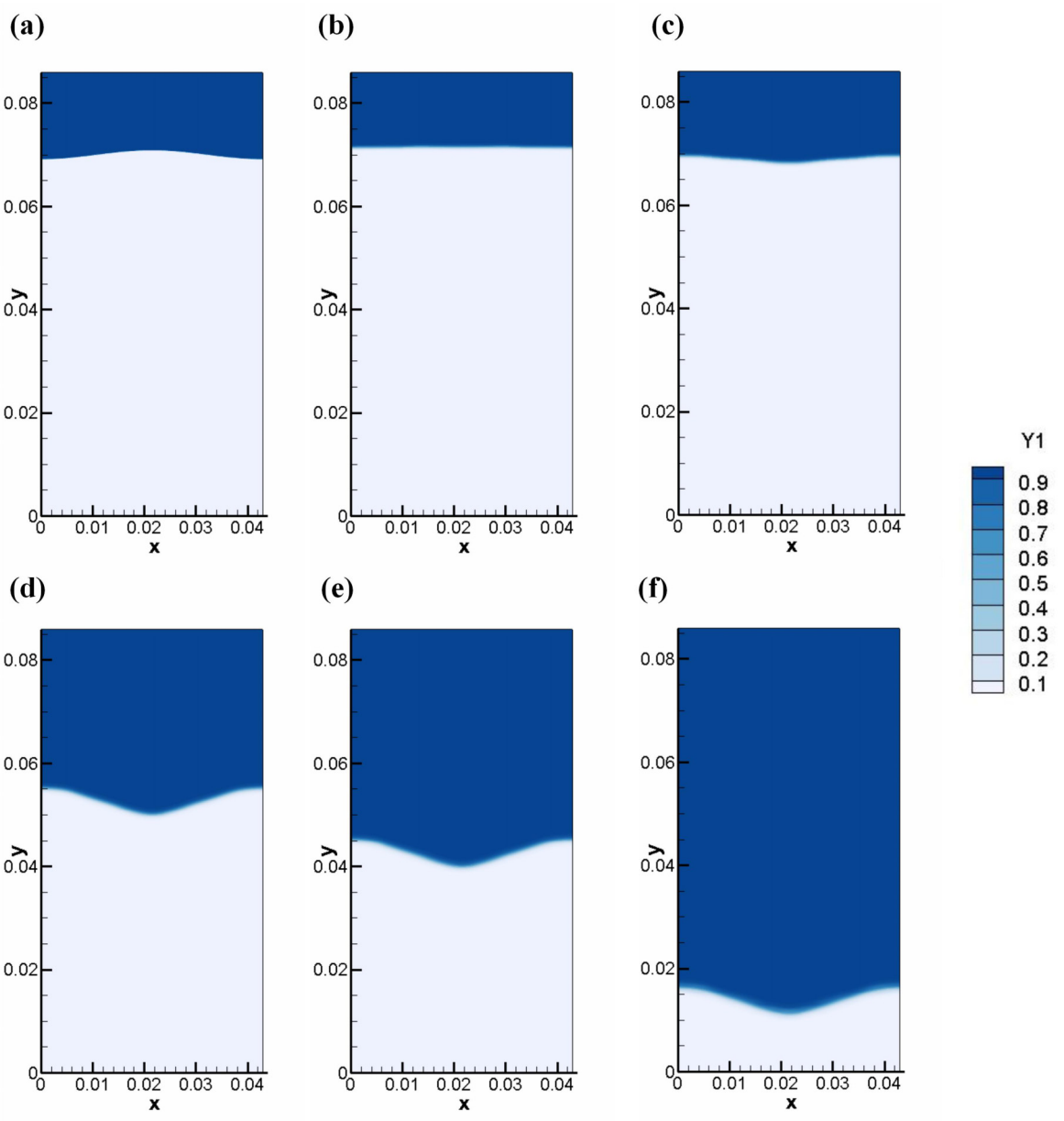

FIG. 4. The interface evolution (A = −0.884) at different stages (volume fraction contours): (a) initial conditions; (b) compression; (c) inversion; (d) tension; (e),(f) long-term behavior.

The results of case 3 are analyzed as an example. The volume fraction contours at different dimensionless times are shown in Fig. 4. The numerical time is scaled by the function $\tau = k\dot{\eta}_0 t$, where τ is the dimensionless time. Similar to the results obtained in the literature [12,23], the growth of small-amplitude perturbations can be divided into three stages. First, the elastic-plastic medium is quickly processed into the plastic state by the loading shock wave. The spike amplitude increases linearly in this state. Then, during the spike growing process, deformation begins to occur in the undeformed material away from the interface. The undeformed region will first enter the elastic state and then change to the plastic state with the growth of the spike. With the expansion of the elastic deformation region, the increasing elastic stress will result in the slowing down of the growth rate of the spikes. In this stage, the elastic properties dominate the above mechanical behavior. The solid adjacent to the interface transitions into an elastic state. The growth rate of the spike nonlinearly decreases to zero. Finally, the interface tends to stabilize. The amplitude of the spike oscillates around an elastic limit related to the material properties of the solid. As shown in the volume fraction contours, the length of the mixing zone tends to a fixed value after the interface is fully developed.

At different postshock Atwood numbers, the profile of the spike amplitude as a function of dimensionless time is shown in Fig. 5. The linear or weak nonlinear growth of perturbations in the early stage is closely associated with the physical evolution, but the slow change of the mixing zone in the long-term behavior is due to the diffusion of the numerical scheme. In this work, the maximum spike

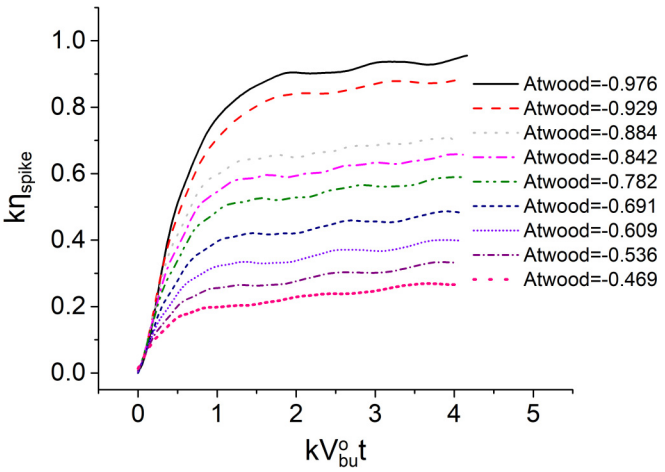

FIG. 5. The profile of the spike amplitude as a function of dimensionless time at different postshock Atwood numbers.

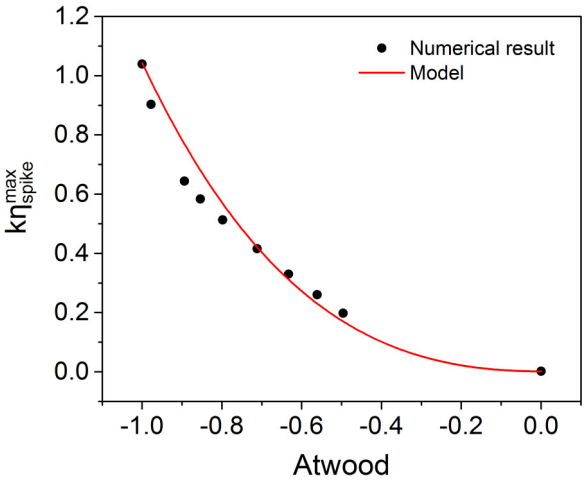

FIG. 6. Comparisons between model profile and numerical results at different Atwood numbers,

length is recorded at the end of the weak nonlinear growth of perturbations, excluding the diffusion stage. The closer the value of the Atwood number gets to 1, the greater the difference in substance densities. As can be seen in Fig. 5, as the Atwood number approaches -1, the linear growth profile of the spike amplitude becomes steep and the maximum spike amplitude also becomes larger, apparently. After the shock travels through the interface, the evolution of the interface can be regarded as a process in which the substance behind the interface accelerates the substance in front of the interface. Therefore, when discussing the effects of Atwood numbers on the spike amplitude, it is assumed that the length of the region moved with the interface is inversely proportional to the total density in the case of the same shock intensity. Moreover, with increasing density of the accelerated liquid, the acceleration will decrease, leading to a decrease in the maximum spike amplitude.

D. Estimation of coefficients and validation of the modified model

By comparing the characteristic statistics collected from the simulation with the modified model, the undetermined model coefficients α and β can be estimated. Firstly, by using the maximum spike amplitude at the solid gas interface ($A = -1$), we can get the constraint between α and β. Thus, the number of the undetermined model coefficients reduces to 1. Furthermore, the value of the coefficient can be estimated by using the relevant characteristic statistics at different Atwood numbers, and it is found to be $\alpha = 0.0034$, $\beta = 3.0374$. By combining with Eqs. (29) and (30), an Atwood number dependent function can be confirmed by the model coefficients and then the model profile of the maximum spike amplitude can be obtained. As shown in Fig. 6, it can be concluded that the consistency of the model profile and numerical results is satisfactory. When $A = -1$, we can get the value of the Atwood dependent function $f(A = -1) = 0.222$, which compares favorably to those from the literature (0.29 in Ref. [12], 0.24 in Ref. [24], 0.22 in Ref. [23]). The model then reduces to

$$k\eta_{\max} = \frac{Y}{4\sqrt{3}G} + f(-1)\frac{\rho_s(k\eta_0\Delta u)^2}{Y} = \frac{Y}{4\sqrt{3}G} + 0.222\frac{\rho_s(k\eta_0\Delta u)^2}{Y}. \quad (34)$$

To verify the applicability of the modified model, the characteristic statistics are collected at different initial conditions and then compared with the model results. This validation process is implemented by comparing the numerical results with those obtained by the model under different initial conditions. As listed in Table III, the initial conditions are adjusted by changing the Atwood numbers and shock speed. Seen in Fig. 7, the blue (solid) line is the model profile of the maximum spike amplitude at the same shock speed as that in Sec. III C while the red (dash dot) line is the model profile when the shock speed is 7000 m/s. The numerical results of the verification cases show good agreement with the model profile. It can be concluded that the modified model is not

TABLE III. Numerical parameters at different verification cases.

Case	ρ_1 (kg/m^3)	ρ_2 (kg/m^3)	Atwood	Shock speed (m/s)	Postshock Atwood
1	8900	1200	−0.762	7640	−0.744
2	8900	8500	−0.023	7640	−0.022
3	8900	500	−0.894	7000	−0.881
4	8900	1000	−0.798	7000	−0.777

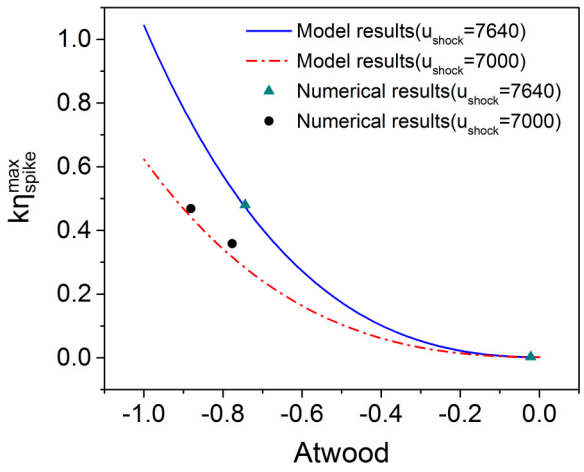

FIG. 7. Model validation under different initial conditions,

only suitable for specific shock intensity and Atwood number, but it also has adaptability in the limit of small perturbations and weak shock conditions.

IV. CONCLUSION

In this work, the effect of Atwood number on the RM instability of the small perturbed interfaces between an elastic-plastic solid and an inviscid liquid is systematically examined. When a shock wave travels through these interfaces, the development of hydrodynamic instabilities in the elastic-plastic solid is induced by the baroclinic effects and governed by the elastic-plastic constitutive properties of the solid. In the case of small perturbations and weak shock limit, the initial perturbations will stop growing when the spike amplitude reaches a maximum value. This phenomenon is mainly attributed to the yield strength of the solid but the maximum spike amplitude is also affected by the density ratios of the media, which is represented by Atwood number. By assuming that the elastic-plastic property can be ignored when the shock wave travels through the interface, the initial growth rate of the interface is considered the same as the linear growth rate of the impulsive model for the fluidic RM instability. After the shock wave travels through the interface, the evolution of the interface can be regarded as a process in which the medium behind the interface accelerates the medium in front of the interface. Thus, the growth rate of initial perturbations will slow down if the absolute value of the Atwood number gets close to 1. Eventually, the spike amplitude reaches a maximum value and remains oscillating due to the elastic property of the solid.

Based on the previous work by Piriz *et al.*, the proposed analytical model at the solid-gas interface is modified to describe the long-time behavior of spike amplitude at different Atwood numbers. The model has two undetermined coefficients, which can be obtained by numerical simulation. Numerical simulation is based on a 2D Eulerian finite-difference multicomponent code. In the numerical results, the linear growth profile of the spike amplitude becomes steep and the maximum spike amplitude grows larger as the Atwood number approaches -1, which is consistent with the theoretical analysis. The constraint between the two undetermined coefficients can be obtained at the case $A = -1$. Therefore, the number of the undetermined model coefficients reduces to 1. By analyzing the relevant characteristic statistics, the last undetermined model coefficient is obtained and the model is completed. Moreover, the applicability of this modified model is verified by comparing the numerical results with the model profile under different initial conditions. The theoretical and numerical results show good agreement; this indicates that this modified model can be used to describe the long-time Atwood number dependent behavior of spike growth in RM instability at small perturbations.

ACKNOWLEDGMENTS

Financial supports from the National Natural Science Foundation of China (Grants No. 91852207, No. 11801036, No. 11502029, No. U1630138, No. U1630247, No. 11872348, and No. 11472059), the China Postdoctoral Science Foundation (Grant No. 2018M641275) and the China Academy of Engineering Physics (Grants No. YZ2015015 and No. TZ2016001) are gratefully acknowledged.

[1] E. E. Meshkov, Fluid Dyn. **4**, 101 (1969).
[2] R. D. Richtmyer, Commun. Pure Appl. Math. **13**, 297 (1960).
[3] K. O. Mikaelian, Phys. Rev. Lett. **80**, 508 (1998).
[4] K. Nishihara, J. G. Wouchuk, C. Matsuoka, R. Ishizaki, and V. V. Zhakhovsky, Philos. Trans. R. Soc., A **368**, 1769 (2010).
[5] Y. Zhou, Phys. Rep. **720–722**, 1 (2017).
[6] Y. Zhou, Phys. Rep. **723–725**, 1 (2017).
[7] M. Lombardini, D. J. Hill, D. I. Pullin, and D. I. Meiron, J. Fluid Mech. **670**, 439 (2011).
[8] W. T. Buttler, D. M. Oró, D. L. Preston, K. O. Mikaelian, and F. J. Cherne, J. Fluid Mech. **703**, 60 (2012).
[9] J. N. Plohr and B. J. Plohr, J. Fluid Mech. **537**, 55 (2005).
[10] A. R. Piriz, J. J. López Cela, N. A. Tahir, and D. H. H. Hoffmann, Phys. Rev. E **74**, 037301 (2006).
[11] A. R. Piriz, J. J. López Cela, M. C. S. Moreno, O. D. Cortázar, N. A. Tahir, and D. H. H. Hoffmann, Nucl. Instrum. Methods Phys. Res., Sect. A **577**, 250 (2007).
[12] A. R. Piriz, J. J. López Cela, N. A. Tahir, and D. H. H. Hoffmann, Phys. Rev. E **78**, 056401 (2008).
[13] D. H. Kalantar, B. A. Remington, J. D. Colvin, K. O. Mikaelian, S. V. Weber, L. G. Wiley, J. S. Wark, A. Loveridge, A. M. Allen, and A. A. Hauer, Phys. Plasmas **7**, 1999 (2000).
[14] Y. Aglitskiy, A. L. Velikovich, M. Karasik, V. Serlin, C. J. Pawley, A. J. Schmitt, S. P. Obenschain, A. N. Mostovych, J. H. Gardner, and N. Metzler, Phys. Rev. Lett. **87**, 265002 (2001).
[15] G. Terrones, Phys. Rev. E **71**, 036306 (2005).
[16] J. J. L. Cela, A. R. Piriz, M. C. S. Moreno, and N. A. Tahir, Laser Part. Beams **24**, 427 (2006).
[17] B. Motl, J. Oakley, D. Ranjan, C. Weber, M. Anderson, and R. Bonazza, Phys. Fluids **21**, 126102 (2009).

[18] A. R. Piriz, J. J. L. Cela, and N. A. Tahir, Nucl. Instrum. Methods Phys. Res., Sect. A **606**, 139 (2009).
[19] J. J. Lopez Cela, A. R. Piriz, and N. A. Tahir, Open Plasma Phys. J. **3**, 80 (2010).
[20] M. T. Henry de Frahan, J. L. Belof, R. M. Cavallo, V. A. Raevsky, O. N. Ignatova, A. Lebedev, D. S. Ancheta, B. S. El-dasher, J. N. Florando, G. F. Gallegos, E. Johnsen, and M. M. LeBlanc, J. Appl. Phys. **117**, 225901 (2015).
[21] M. B. Prime, W. T. Buttler, M. A. Buechler, N. A. Denissen, M. A. Kenamond, F. G. Mariam, J. I. Martinez, D. M. Oró, D. W. Schmidt, and J. B. Stone, J. Dyn. Behav. Mater. **3**, 1 (2017).
[22] A. López Ortega, D. J. Hill, D. I. Pullin, and D. I. Meiron, Phys. Rev. E **81**, 066305 (2010).
[23] A. López Ortega, M. Lombardini, D. I. Pullin, and D. I. Meiron, Phys. Rev. E **89**, 033018 (2014).
[24] G. Dimonte, G. Terrones, F. J. Cherne, T. C. Germann, V. Dupont, K. Kadau, W. T. Buttler, D. M. Oro, C. Morris, and D. L. Preston, Phys. Rev. Lett. **107**, 264502 (2011).
[25] G. Dimonte, R. Gore, and M. Schneider, Phys. Rev. Lett. **80**, 1212 (1998).
[26] K. O. Mikaelian, Phys. Rev. E **87**, 031003(R) (2013).
[27] A. R. Piriz, Y. B. Sun, and N. A. Tahir, Phys. Rev. E **88**, 023026 (2013).
[28] A. L. Ortega, M. Lombardini, P. T. Barton, D. I. Pullin, and D. I. Meiron, J. Mech. Phys. Solids. **76**, 291 (2015).
[29] A. R. Piriz, Y. B. Sun, and N. A. Tahir, Phys. Rev. E **91**, 033007 (2015).
[30] Q. Zhang and W. Guo, J. Fluid Mech. **786**, 47 (2016).
[31] A. R. Piriz, J. J. López Cela, O. D. Cortázar, N. A. Tahir, and D. H. H. Hoffmann, Phys. Rev. E **72**, 056313 (2005).
[32] J. J. López Cela, A. R. Piriz, M. Temporal, N. A. Tahir, and M. C. S. Moreno, Eur. Phys. J. Appl. Phys. **29**, 247 (2005).
[33] A. R. Piriz, J. J. López Cela, and N. A. Tahir, Phys. Rev. E **80**, 046305 (2009).
[34] A. R. Piriz, J. J. L. Cela, and N. A. Tahir, J. Appl. Phys. **105**, 116101 (2009).
[35] A. R. Piriz, Y. B. Sun, and N. A. Tahir, Phys. Rev. E **89**, 063022 (2014).
[36] Y. B. Sun and A. R. Piriz, Phys. Plasmas **21**, 072708 (2014).
[37] S. A. Piriz, A. R. Piriz, and N. A. Tahir, Phys. Rev. E **95**, 053108 (2017).
[38] S. A. Piriz, A. R. Piriz, and N. A. Tahir, Phys. Rev. E **96**, 063115 (2017).
[39] A. Subramaniam, N. Ghaisas, and S. K. Lele, J. Fluids Eng. **140**, 050904 (2017).
[40] J. G. Wouchuk, Phys. Rev. E **63**, 056303 (2001).
[41] M. Lombardini and D. I. Pullin, Phys. Fluids **21**, 044104 (2009).
[42] J. W. Swegle and A. C. Robinson, J. Appl. Phys. **66**, 2838 (1989).
[43] A. C. Robinson and J. W. Swegle, J. Appl. Phys. **66**, 2859 (1989).
[44] M. B. Liu, G. R. Liu, K. Y. Lam, and Z. Zong, Comput. Mech. **30**, 106 (2003).